

INVESTIGATION OF SIZE AND BAND GAP DISTRIBUTIONS OF SI NANOPARTICLES FROM MORPHOLOGY AND OPTICAL PROPERTIES OF POROUS SILICON LAYERS FORMED ON A TEXTURED N⁺ P SILICON SOLAR CELL

G. M. YOUSSEF¹, M. M. EL-NAHASS², S. Y. EL-ZAIAT³ & M. A. FARAG⁴

¹Department of Physics, Faculty of Science, Ain Shams University, Abbassia, Cairo, Egypt

²Department of Physics, Faculty of Education, Ain Shams University, Heliopolis, Cairo, Egypt

ABSTRACT

Fabrication of PS layers (PSLs) was performed by electrochemical etching process on the front side of textured n⁺p Si junctions. The structural and optical properties of the treated textured cells were investigated and compared with the untreated textured cell under the variation of etching current densities. Surface morphology and the crystallites size of PS were characterized by using scanning electron microscope (SEM) and X-ray diffraction (XRD), respectively. The porosity of the PSLs was determined gravimetrically and it was dependent on etching current density. The reflection measurements showed an excellent light trapping at wavelengths ranging from 200 to 1000 nm at 30 mA/cm² etching current density. The optical absorption coefficient was calculated from the reflection spectra and the optical band gap was determined. The value of the energy gap (E_g) was also determined by applying the Kubelka-Munk (K-M or F(R)) method. From the photoluminescence (PL) measurements, the PL peak intensity increases upon increasing the porosity and also shows slight blue shifts at 629 nm and 640 nm as the porosity increases. The band gaps of PSLs obtained from the photoluminescence measurements and from the reflection data were compared. It is found that the band gap increases in a range between 1.84 eV and 2.23 eV, which is higher than the band gap of silicon (1.12 eV). It is obtained that the fabrication of the solar cells based on the PS anti-reflection coating (ARC) layers exhibited its high performance to enhance and increase the photo-conversion process and increasing light absorption at 30 mA/cm² etching current density.

KEYWORDS: Porous Silicon, XRD, SEM, ARC, Solar Cell, PL, Band Gap

Original Article

Received: Dec 03, 2015; **Accepted:** Dec 10, 2015; **Published:** Dec 18, 2015; **Paper Id.:** IJSSTFEB20161

INTRODUCTION

Photovoltaic industry is currently ruled by silicon solar cells technology. Because of its wide use in solar energy, there is a need of creating new technologies and materials processes in which porous silicon is expected to be promising for modifying the silicon surface [1]. The discovery of porous silicon (PS) by Uhlir in 1956 [2] opened the door for new applications in micro-and optoelectronics, such as chemical sensors, sacrificial/separation layers, light emitting diodes and passive optical filters [3]. PS was intensely studied since it was reported for visible photoluminescence by Canham in 1990[4, 5] because porous silicon layer acts as an ultra efficient anti-reflection coating for solar cells with high absorption in visible spectrum regions[1, 6]. PS is also used as smart transducer material for sensing applications for the detection of vapors, liquids and biochemical molecules[7-10]. The promising way to overcome the reflectance losses and increasing the surface area of the

solar cell is by texturing the cell surface which could be done by several techniques. The most popular technique for texturing the cell surface is the electrochemical etching.

The texturing of the solar cell surface could enhance the optical, electrical and also the conversion efficiency of the cell [11-14, 6]. PS can be obtained conventionally by anodization of silicon substrates. Crystallites of silicon formed by these ways have diameters varying from units of nanometers to tens of micrometers, depending on formation parameters (current density, electrolyte concentration, etching time and substrate type)[15]. The quantum confinement effects are considered to control the mechanism of the luminescence in nanocrystallites[16, 17]. The reduction of particle size to a few nanometers is necessary to detect efficient light emission as it modifies the electronic, optical and vibration properties [18]. The significant characteristics of visible PL in PSLs at room temperature have given great desire to material studies due to the vast possibilities for technological applications [19, 20].

Three mechanisms have carefully been discussed in the literature as being responsible for the various PL features reported in PSLs [21-23]. The commonly accepted PL mechanism is the quantum size effect (QSE), which is maintained by the nanometric dimensions of the filaments constituting the PSLs [24]. When reducing the size of nanoparticles in PS, the bandgap increases and due to relaxation of the quasimomentum selection rule, the probability of optical transitions significantly increases, which leads to increased intensity and shift of the PL spectra to the visible region[25]. A second mechanism is correlated to the siloxene-like film that covers the porous silicon structured net[26]. Besides, the non-stable behavior of PL has been correlated to some kind of interfacial states located between the silicon filaments and the siloxene-like surface film [27]. The interface between the phenomena mentioned must be taken into account for the utilizing of PSLs in technological applications. PSLs prepared by several techniques show different features in their PL spectra, but the work discussing the relative influence of the different mechanisms is restricted [28].

Morphology is the minimum quantifiable aspect of a material which is obtained by the distribution of matter in space. Therefore, it is very difficult to systematically characterize morphology of PS, which has exceedingly rich details with respect to the range of variations in pore size, shape, orientation, branching, interconnection, and distribution [29]. In addition, the material characteristics and applications of porous silicon depend on its microstructure which can be described by a large number of parameters [30-33]. The porosity and thickness are the key properties affecting the optical, mechanical, thermal, chemical and electrical characteristics of porous silicon [34]. The advantages of PS, such as the possibility of broadening of the bandgap, large active area for the light-semiconductor interaction, decrease of reflection losses, the specific character of its absorption spectrum, their rough surface and low effective refractive index compared to c-Si, etc., lead to an increase in the photovoltaic properties of solar cells [35]. Many experiments indicated that the characteristics of silicon solar cells can be enhanced by coating the n^+ emitter region with PS; in fact, it was revealed that the structural and optical properties of PS enable good electrical passivation and low surface recombination velocity[36]. Furthermore, porous silicon is used to passivate and getter impurities in crystalline silicon substrates [37-39] and (600-800 nm) light emission properties [5]. Therefore, in this work, the aim of this study is to determine the size and bandgap distributions of silicon nanoparticles from the reflection measurements and the photoluminescence spectra. Moreover, we have presented the effects of the effective parameters on the surface morphology obtained by using SEM and related the results with the calculated values of the size and bandgap distributions of silicon nanoparticles. Our study related the obtained results of the characteristics of these PSLs structures with their electrical properties which also has been demonstrated and confirmed in a previous work [6].

EXPERIMENTAL TECHNIQUES AND SAMPLE PREPARATION

Textured n⁺ p junction silicon solar cells of a thickness of 450 μm which have a resistivity of 4-5 Ωcm and (100) orientation of CZ crystalline silicon wafers were used in this study. Porous silicon technology operations were carried out in the electrochemical cell. The used electrochemical cell has two electrode configurations with a platinum electrode as cathode and silicon wafer as anode. Etching of only one side of the solar cell has been considered in this design, while the backside of the solar cell is absolutely separated from the etching acid. Before the etching process, silicon wafers have been submerged into de-ionized water followed by heating in isopropyl for 5 minutes. Production of porous silicon layer has been done in the etching solution containing HF (48%): C₂H₅OH (98%) = 1:4 by volume ratio electrolytes with different etching current densities on the front side of n⁺ p Si junctions. The mixing of ethanol in electrolyte solution is helpful to improve the lateral homogeneity and the uniformity of the porous silicon layer by promoting the hydrogen bubble removal [40].

Three samples A, B, C of porous silicon layer were prepared at 10, 20 and 30 mA/cm² for constant etching time of 10min. After the etching process, the samples have been cleaned by immersion in acetone and then immersed in ethanol to clean off the acetone residue. Afterwards, the samples were dried under nitrogen gas flow. The surface morphology and roughness of prepared samples were characterized by using scanning electron microscopy (SEM) (Model Quanta 250 FEG). X-ray diffraction (XRD) measurements were carried out using a high-resolution X-ray diffractometer system (Philips-mpw1840 supplied from Philips company) utilizing a CuK α radiation with a wavelength of 0.15406 nm. The total optical reflectance of the C-Si sample and PSLs were obtained using an optical reflectometer (JASCO V-570) which is equipped with an integrating sphere [6]. The photoluminescence was measured by using a monochromator (Jobin Yvon) with an attached charge coupled device. A beam of 325nm line from argon laser at 10mW output power was used for excitation.

RESULTS AND DISCUSSIONS

X-Ray Diffraction

Figure 1 represents the XRD patterns for the PS layers fabricated at different etching current density: A, B, C together with the XRD pattern of the as grown C-Si. The patterns show a strong peak which is corresponding to the growth along (100) direction of crystalline silicon. The different surface morphologies of the PS samples A, B, C fabricated with dissimilar etching techniques obtain different diffraction angles of different shapes on the porous layers [41]. The matching between the theoretical part and experimental part can be investigated depending on different types of porosity which aids to calculate the grain size [42].

The average grain size (crystallite size) was calculated using the Debye–Scherrer formula expressed as [43]:

$$D = \frac{0.9\lambda}{B \cos\theta} \quad (1)$$

where λ is the X-ray radiation wavelength (0.15406 nm), B is the full width at half maximum of the peak intensity and θ is the diffraction Bragg's angle. The values of the crystallite size of the C-Si and the PS samples are shown in Table 1. It can be observed that the grain size decreases with increasing etching current density.

The reduction in the crystallite size can be deduced through the increase in broadening of the XRD spectra, also, suggests that there is an increase in the porosity of the PS layer [41]

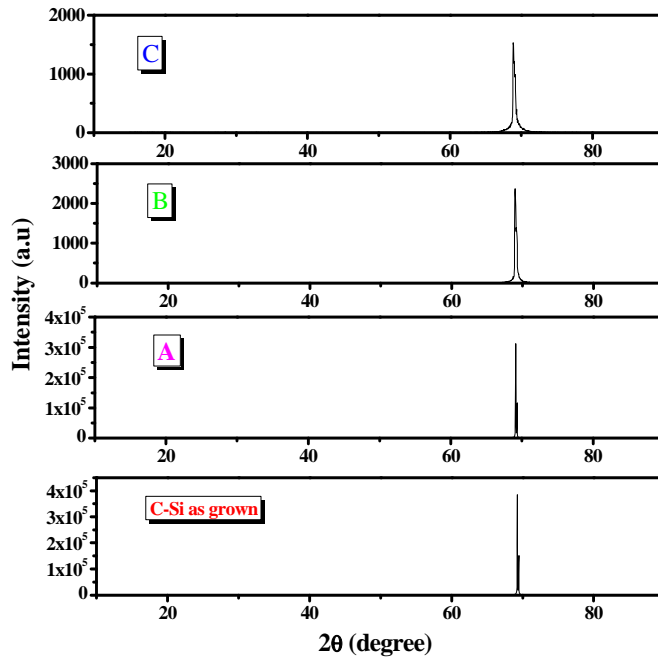


Figure 1: The XRD Results for the Unetched Si Sample Compared with the Etched Sample Fabricated at Different Current Densities: A, B and C

Table 1: The Average Crystallite Size of the Bulk Silicon Compared with the PS Samples Fabricated at Different Etching Current Densities: A, B and c

Sample	20°	FWHM (20°)	Average Crystallite Size (nm)
Reference C_Si	68.784°	0.33	24.07
A	69.088°	0.445	19.01
B	68.863°	0.423	18.73
C	68.784°	0.576	16.72

Morphological Characteristics

Figure 2(a-d) shows the SEM images of the front surface of the solar cell before and after etching. The surface morphology of the textured untreated substrate shows different sizes of spaced pyramids distributed on the whole surface as shown in Figure 2(a). For sample A, the results show that etching produces pits, which randomly spread over the surfaces of pyramids. With the increase of the current density up to C, the pyramids became blunt and started to collapse. With further increase of the current density to C, the pyramids are completely collapsed and the roughness of the surface has increased. Generally, it can be said that the whole surfaces of the samples are completely etched and that there is an obvious increase in surface area due to the regular porosity and pore size distribution in different locations on the pyramids.

The obtained surface images are more indicated with the cross-sectional view SEM micrograph as shown in Figure 3(a-d). The images confirm the change in the morphology and in the PSL thickness with changing porosity. The pore formation occurs in a unidirectional manner from the surface into the bulk, leading to aligned pores and columnar silicon structures. In addition, it is observed that the average PS layers thickness increases in which their values are listed in Table 2.

Table 2: The Experimental Values of the Parameters (Thickness (μm), Porosity (%), Pore Diameter (Nm) of the PS Samples Fabricated at Different Etching Current Densities: A, B and C

Sample	Thickness (μm)	Porosity (%)	Pore diameter (nm)
A	7.99	88.27	5.90
B	10.09	95.00	5.86
C	13.70	97.00	5.82

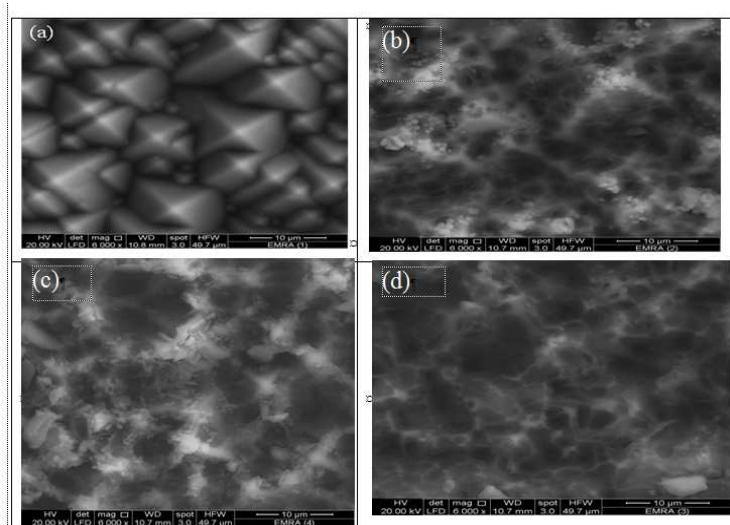


Figure 2: SEM Image of (A) The Unetched Crystalline Si Sample and for the Etched Samples Under Different Etching Current Densities: (B): A, (C): B and (D): C

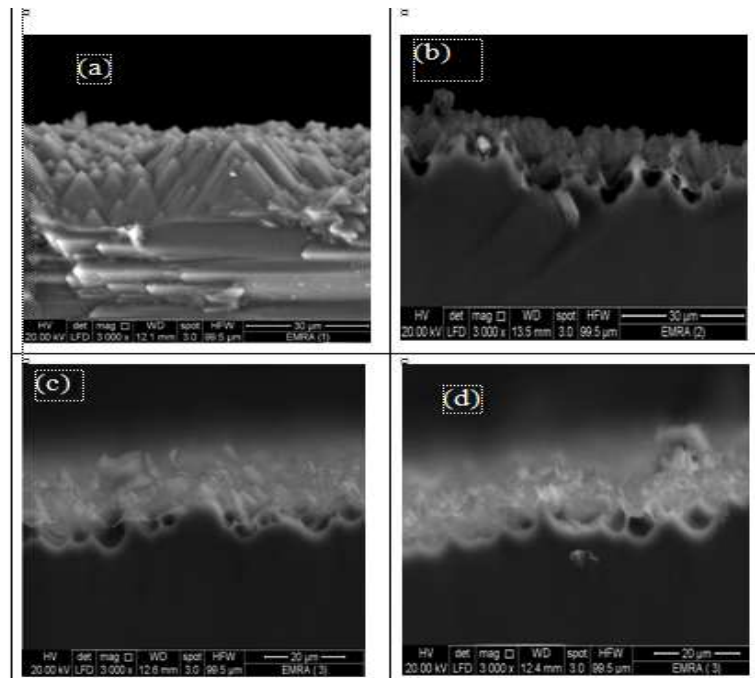


Figure 3: Cross-Section Semimages of (A) The Unetched Crystalline Si Sample and for the Etched Samples under Different Current: (B): A, (C): B and (D): C

Gravimetical Measurements

The change in the surface morphology and the thickness of the PSLs is an evidence of the variation in the

percentages of porosity in each sample depending on the anodizing conditions. The porosity was calculated by using the gravimetric method according to the following equation [44]:

$$P(\%) = \frac{m_1 - m_2}{m_1 - m_3} 100\% \quad (2)$$

where m_1 is the sample weight before anodization, m_2 is the sample weight after anodization and m_3 is the sample weight after removing the PS layer with a 3% KOH solution in 50 sec times [45]. The porosity of the PSL produced was found in the high range between 88.27 – 97.00 % [6]. It is also observed that the porosity increases with increasing etching current density as presented in Table 2. Hence, the variation of porosity is positively related to the thickness of PSLs and in accordance with the results obtained from SEM.

Optical Properties

Figure 4 shows the diffused reflectance spectra for the samples after formation of a PS layer on the front surface of C-Si solar cells compared with the as-grown Si sample in the wavelength region of 200 to 1100 nm[6]. In the range of 200 to 550 nm, there is a significant decrease of the reflectivity for the sample A compared to the untreated PS structure. More reduction in the reflectivity occurs by increasing the etching current to B in the wavelength range 200 to 750nm with a minimum value of reflection about 7%. At larger anodization (C), the reflectance satisfied maximum reduction in light reflection in the wavelength range 200 to 800 nm reaching a minimum value of about 4% compared to the untreated C-Si solar cell. It is also observed that there is a slight increase in the reflection in spectral ranges 800 to 1000 nm, which could be caused from the random distribution of the pores and the high roughness degree on the PS textured surfaces

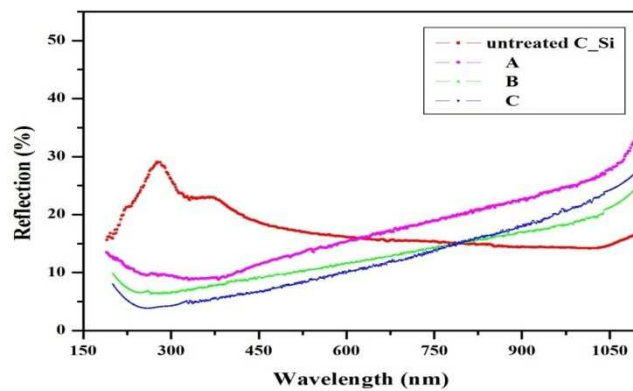


Figure 4: Reflection Spectra of the As-Grown Si compared with the PS Samples Fabricated at Different Etching Current Densities A, B and C

The attenuation of the reflectivity is due to trapping effect. Moreover, this demonstrates that the lowest effective specular reflectance was verified from the PSL at 30 mA/cm² etching current density, which obviously reduced the light reflection and increased the light-trapping, hence it plays an important role for improvement of the solar cell efficiency.

The results of the diffused reflectance measurements are very important for determination of the absorption coefficient which can be calculated by using the following expression [46]:

$$\alpha = \frac{1}{2t} \ln \frac{(R_{\max} - R_{\min})}{(R - R_{\min})} \quad (3)$$

where t is the film thickness, R_{\max} and R_{\min} are the maximum and minimum reflectance in the diffused reflection spectra and R is the reflectance for any intermediate energy photons recorded by the spectrophotometer.

The value of absorption coefficient (α) near band edge provides key information about the film's band structure. The energy gap can be determined from the well-known relation [47]:

$$\alpha h\nu = A(h\nu - E_g)^m \quad (4)$$

where (A) is the edge width parameter and (E_g) is optical energy gap of the material. The parameter (m) represents the type of transition. For direct transition ($m=1/2$) and for indirect transition ($m=2$). The usual method for the determination of the value of (E_g) involves a plotting of $(\alpha h\nu)^{1/2}$ versus $(h\nu)$ and it can be obtained from the intercept of extrapolation to zero absorption with the photon energy axis. The plot of $[\alpha h\nu]^{1/2}$ versus $(h\nu)$ for PS samples with different etching current densities compared with the C-Si as grown is presented in Figure 5. It can be observed that there is blue shift in the optical band gap because of increasing the etching current density, which can be explained by the quantum size effect [48, 49]. The values of E_g of the samples are presented in Table 3.

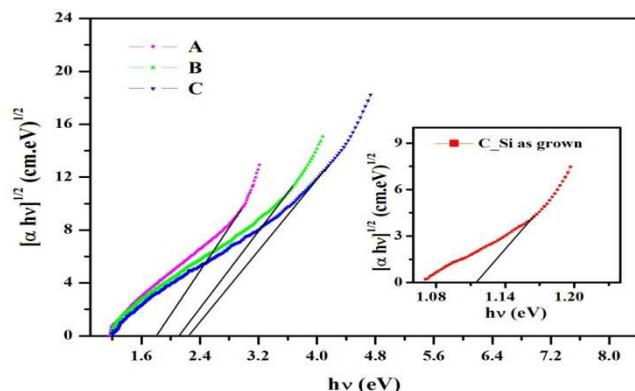


Figure 5: $[\alpha h\nu]^{1/2}$ Versus $h\nu$ for Indirect Allowed Transition of the as Grown Si in the Inset Compared with the PS Samples with Different etching Current Densities A, B, and C

Furthermore, Kubelka–Munk proposed an additional method to determine the optical energy gap from the specular reflectance measurements according to the following function [50, 51]:

$$F(R) = \frac{(1-R)^2}{2R} \quad (5)$$

where the function $F(R)$ is proportional to the extinction coefficient (α), by plotting the relation between $[F(R) * h\nu]^{1/2}$ versus $(h\nu)$, the band gap of semiconductor particles can be obtained from the extrapolation of the linear behavior $[F(R) * h\nu]^{1/2}$ towards $(h\nu)$ axis at $F(R) = 0$. Figure 6 shows a perfect fit obtained for all the samples giving the optical band gap values of 1.12 eV for the as grown C-Si. These values increased to 1.8, 2 and 2.2 eV for the PS samples A, B, C, respectively. These results are summarized in the Table 3.

Table 3: The Calculated Band Gaps Obtained From UV-Vis-NIR and PL Measurements of the Bulk Silicon compared with the PS Samples Fabricated at Different Etching Current Densities A, B, and C

Sample	Band Gap (eV)		
	UV-Vis-NIR		PL
	$[\alpha h\nu]^{1/2}$ Vs $h\nu$	$[F(R)h\nu]^{1/2}$ Vs $h\nu$	I_{PL} Vs λ
C-Si	1.11	1.06	1.12(literature) [56]
A	1.81	1.75	1.89
B	2.08	1.94	1.90
C	2.25	2.20	1.91

The refractive index n is important in the advancement of different materials in optoelectronic research. Therefore, n as a function of wavelength is an important parameter and should be evaluated for the design of various devices, such as integrated optical switches, filters, and modulators. Efforts have been devoted to relate n to energy gap (E_g) based on simple relationships [52–56]. In the present study, various relationships between n and E_g were reviewed. Ravindra et al. [56] suggested that different relationships are present between band gap and high-frequency n , in which a linear form of n as a function of E_g is presented as follows:

$$n = \alpha + \beta E_g \quad (1)$$

where $\alpha = 4.048$ and $\beta = -0.62 \text{ eV}^{-1}$.

Moreover, light refraction and dispersion are also considered. Hervé and Vandamme [57] proposed an empirical relationship as follows:

$$n = \sqrt{1 + \left(\frac{A}{E_g + B}\right)^2} \quad (2)$$

where $A = 13.6 \text{ eV}$ and $B = 3.4 \text{ eV}$.

For group IV semiconductor, Ghosh et al. [58] showed an empirical relationship based on the band structure and quantum dielectric considerations of Penn [59] and VanVechten:

$$n^2 - 1 = \frac{A}{(E_g + B)^2} \quad (3)$$

where $A = 25E_g + 212$, $B = 0.21E_g + 4.25$, and $(E_g + B)$ refers to an appropriate average optical energy gap of the material.

The calculated n of the end-point compounds are determined from the values of E_g calculated from Figure 5 are listed in table 4.

These results are verified by calculating the optical dielectric constant ϵ_∞ , which is dependent on n ; hence, $\epsilon_\infty = n^2$ [60]. The n obtained using the Hervé and Vandamme model [56] is important to enhance the detecting and sensing of porous silicon nanostructure. Therefore, high absorption may be attributed to an increase in sensor efficiency.

Table 4: Calculated Refractive Indices for PS Using Ravindra et al. [56], Herve and Vandamme [57] and Ghosh et al. [58] Models Compared with Others Corresponding to Optical Dielectric Constant. (A Ref. [56], B Ref. [57] in Addition, C Ref. [58])

Sample	E _g (eV)	n	ε _∞
A	1.81	2.95, 2.79 ^b , 2.68 ^c	8.748 ^a , 7.81 ^b , 7.20 ^c
B	2.08	2.79 ^a , 2.67 ^b , 2.52 ^c	7.78 ^a , 7.16 ^b , 6.37 ^c
C	2.25	2.68 ^a , 2.60 ^b , 2.55 ^c	7.21 ^a , 6.76 ^b , 5.52 ^c

Photoluminescence Spectroscopy

Figure 6 shows the room temperature photoluminescence (PL) spectra of the etched samples at different current densities. It is observed that there is an emission peak in the spectral range 648-652 nm.

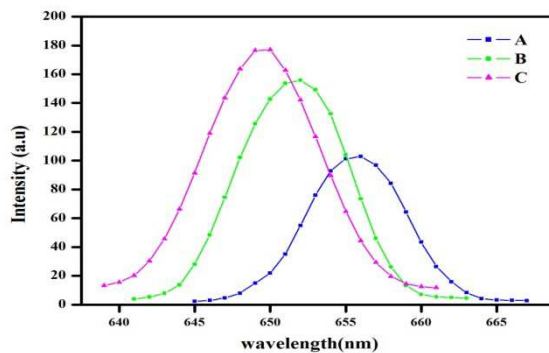


Figure 6: PL Spectra of PS Layers Fabricated at Different Etching Current Densities A, B and C

The PL intensity increases with increasing etching current density and the maximum intensity is obtained at sample C. It can be seen that PL maximum shifts slightly to lower wavelengths with increasing etching current density. Then, from the PL spectrum, the energy gap was determined by equation [4]:

$$E_g = \frac{hc}{\lambda} \quad (7)$$

where E_g is energy gap of the PS, h is Planck constant, c is the speed of light and λ is the peak wavelength of the photoluminescence. The energy band gap was found to increase from 1.12 eV for the c-Si sample to 1.89, 1.9 and 1.91 eV for the PS layer fabricated A, B and C mA/cm² etching current density, respectively, as seen in Table 3. The increase in the energy band gap confirms that there was a blue shift in the maximum PL intensity. Broadening of the band gap energy occurs when there is a decrease in the crystallite size [61]. In addition, this means that the particles are confined into lower dimension and the probability of the recombination of the electrons and holes is higher in low dimensional structures according to quantum confinement effects [62,63]. This lead to high efficiency and energy. The average pore diameter is calculated by the following equation [64]:

$$E(\text{eV}) = E_g + \frac{h^2}{8d^2} \left[\frac{1}{m_e^*} + \frac{1}{m_h^*} \right] \quad (8)$$

where E (eV) is the energy band gap of PS calculated from the PL peak position of the PS layer as shown in Figure 6, E_g = 1.12 eV is the energy band gap of bulk Si, h is Planck's constant = 4.13 x 10⁻¹⁵ eV s and m_e^{*}, m_h^{*} are the electron and hole effective mass, respectively (at 300 K, m_e^{*} = 0.19m_o, m_h^{*} = 0.16m_o where m_o = 9.109 x 10⁻³¹ Kg) [65]. The resultant values of (d) for all the PS samples are calculated and summarized in Table 2.

CONCLUSIONS

By using electrochemical etching method, porous silicon structures are fabricated with different current densities (10, 20 and 30 mA/cm²). The effect of the different etching times on the characteristics of these PS structures has been observed. The results showed that as the current density increases the pore size, physical thickness of the porous layer, porosity, and energy band gap increase. Moreover, the broadening of the FWHM obtained from the XRD spectra provided the reduction in the crystallite size. This means that this technique has promising great control over the final shape and size of the resultant PS nanostructure. In addition, the intensity peak of photoluminescence of porous silicon layers was found to increase with increasing current density. All these parameter is important in enhancing the photo conversion process and the photovoltaic parameters for solar cell devices as we confirmed in our previous study [6]. The results also showed that the optimal etching current density to prepare the PS is 30 mA/cm², which can be used to enhance and increase the photo conversion process and increasing light absorption compared with other etching current densities and that of the as-grown Si. We indicate that PS layers formed on textured surface for can be used as both broadband antireflection coatings and passivation layers for the application in solar cells.

REFERENCES

1. R. S. Dubey, D. K. Gautam, *Journal of optoelectronic and biomedical materials* 1 (2009): 8-14.
2. A Uhlir, Jr., *Bell Syst. Tech. J.* 35 (1956): 333-347.
3. H. Foll, M. Christophersen, J. Carstensen, *Mat. Sci. and Eng.* 39 (2002): 94-141.
4. D. T. J. Ee, C. K. Sheng, *Malaysian Journal of Analytical Sciences* 15 (2011) :227-231.
5. L. T. Canham, *Appl. Phys. Lett.* 57 (1990); 1046-1048.
6. G. M. Youssef, M. M. El-Nahass, S. Y. El-Zaiat, M. A. Farag, *Mater. Sci. Semicond. Process.* 39 (2015) ;457-466.
7. S. Singh, S. N. Sharma, S. M. Shivaprasad, *J. Mater. Sci.: Mater.* 20 (2009) :181-187.
8. L. Moretti, I. Rea, L. De Stefano, *Appl. Phys. Lett.* 90 (2007) 191112.
9. E. Descrovi, F. Frascella, B. Sciacca, *Appl. Phys. Lett.* 91 (2007) 241109.
10. H. Ouyang, C. C. Striemer, P. M. Fauchet, *Appl. Phys. Lett.* 88 (2006) 163108.
11. A. Laugier, J. A. Roger, *Les photopiles solaires, du materiel au dispositif, du dispositif aux applications, Technique et documentation*, (1981) 139.
12. J. Xiao, L. Wang, *Applied Surface Science* 257 (2010) :472-475.
13. O. Weiying, Z. Lei, *Journal of Semiconductors* 32 (2011) 056002.
14. A. Ramizy, M. A. Mahdi, *Applied Surface Science* 257 (2011): 6112-6117.
15. U. Nayef, *International Journal of Basic and Applied Sciences* 13 (2013) 61.
16. M. Voos, Ph. Uzan, C. Delalande, G. Bastard, *Appl. Phys. Lett.* 61 (1992) 1213.
17. S. M. Prokes, J. A. Freitas, P. C. Searson, *Appl. Phys. Lett.* 60 (1992) 3295.
18. R. L. Smith, S. D. Colline, *J. Appl. Phys.* 71 (1992) R1-R22.
19. B. C. Chakravarty, J. Tripathi, A. K. Sharma, *Sol. Energy Mater. Sol. Cells.* 91(2007):701-706.

20. G. Romero-Paredes, R. Pe`na-Sierra, G. Castillo-Cabrera, *Rev. Mex. Fis.* 48 (2002):92-99.
21. R. Tsu, H. Shen, M. Dutta, *Appl. Phys. Lett.* 60 (1992) 112.
22. V. Lehmann, U. G. Gosele, *Appl. Phys. Lett.* 58 (1991) 856.
23. W. L. Wilson, T. Weidman, *J. Phys. Chem.* 95 (1991) 4568.
24. G. C. John, V. A. Singh, *Phys. Rev. B.* 50 (1994) 5329.
25. F. A. Rustamovn, N. H. Darvishov, *Journal of Luminescence* 154 (2014) :224–228
26. M. Koos, Y. Pocsik, E. B. Vazsomyi, *Appl. Phys. Lett.* 62 (1993) 1797.
27. H. J. Lee, *J. Appl. Phys.* 75 (1994): 8060-8065.
28. A. N. Chifan, W. Knoll, R. Forch, *Mater. Lett.* 61 (2007) 1722.
29. X. G. Zhang, *J. Electrochem. Soc.* 151(2004): 69-80.
30. N. Naderi, M. R. Hashim, *Mater. Sci. Semicond. Process.* 16 (2013); 542–546.
31. G. L. Liu, P. Y. Dai, Y. Z. Wang, J. F. Yang, Y. B. Zhang, *J. Eur. Ceram. Soc.* 31 (2011): 847–854.
32. Y. S. Zhang, Z. M. Yang, D. L. Liu, *J. Lumin.* 130 (2010) :1005–1010.
33. A. M. Giovannozzi, C. Renacco, *Phys. Status Solidi C* 8 (2011) :1878–1882.
34. S. Lazarouk, P. Jaguiro, *Thin Solid Films* 297 (1997): 97–101.
35. Z. N. Adamian, V. M. Aroutiounian, *Solar Energy Materials & Solar Cells* 64 (2000) :347-351
36. M. Ben Rabha, B. Bessaïs *Solar Energy* 84 (2010) :486–491
37. L. Derbali, W. Dimassi, H. Ezzaouia, *EnergyProcedia* 10(2011) :243–248.
38. M. Hajji, M. Hassen, H. Ezzaouia, A. Selmi, H. Bouchriha, *Applied Surface Science* 253 (2007) :5341–5344.
39. D. Lotfi, E. Hatem, *Nanoscale Research Letters* 7(2012) 338.
40. R. S. Dubey, D. K. Gautam, *Chalcogenide Letters* 6 (2009) :523-528.
41. A. Ramizy, Z. Hassan, K. Omar, *J Mater Sci: Mater Electron* 22 (2011) :717–723.
42. K. Omar, Y. Al-Douri, *Superlattices and Microstructures* 50 (2011) :119–127.
43. B. D. Cullity, *Elements of X-ray Diffraction*, Addison-Wesley, London, (1959).
44. L. Hyunwoo, E. Lee, L. Soohong, NMDC. IEEE, Gyeongju, Korea. (2006):340–341.
45. S. FaY, A. Shah, In: *Transparent Conductive Zinc Oxide*. Springer, Berlin Heidelberg. (2008):235–302.
46. V. Kumar, S. K. Sharma, *Opt. Mater.* 12 (1999: 115-119.
47. A. Mortezaali, S. R. Sani, F. J. Jooni, *Journal of Non-Oxide Glasses* 1 (2009):293-299.
48. L. T. Canham (ed.), *Properties of Porous Silicon*” INSPEC, London, (1997): 349.
49. A. G. Cullis, L. T. Canham, *J. Appl. Physics.* 82 (1997).
50. P. Kubelka, F. Munk, *Z. Tech. Phys.* 12 (1931) 593.
51. P. Kubelka, *J. Opt. Soc. Am.* 38 (1948) 448.

52. T. S. Moss, "A relationship between the refractive index and the infra-red threshold of sensitivity for photoconductors," *Proceedings to the Physical Society B*, vol. 63, no. 3, article 302, pp. 167–176, 1950.
53. V. P. Gupta and N. M. Ravindra, "Comments on the mossformula," *Physica Status Solidi B*, vol. 100, no. 2, pp. 715–719, 1980.
54. P. Hervé and L. K. J. Vandamme, "General relation between refractive index and energy gap in semiconductors," *Infrared Physics and Technology*, vol. 35, no. 4, pp. 609–615, 1994.
55. H. J. Fan, R. Scholz, F. M. Kolb et al., "On the growth mechanism and optical properties of ZnO multi-layer nanosheets," *Applied Physics A*, vol. 79, no. 8, pp. 1895–1900, 2004.
56. N. M. Ravindra, S. Auluck, and V. K. Srivastava, "On the penn gap in semiconductors," *Physica Status Solidi B*, vol. 93, no. 2, pp. K155–K160, 1979.
57. P. J. L. Hervé and L. K. J. Vandamme, "Empirical temperature dependence of the refractive index of semiconductors," *Journal of Applied Physics*, vol. 77, no. 10, pp. 5476–5477, 1995.
58. D. K. Ghosh, L. K. Samanta, and G. C. Bhar, "A simple model for evaluation of refractive indices of some binary and ternary mixed crystals," *Infrared Physics*, vol. 24, no. 1, pp. 43–47, 1984.
59. D. R. Penn, "Wave-number-dependent dielectric function of semiconductors," *Physical Review*, vol. 128, no. 5, pp. 2093–2097, 1962.
60. Samara GA: Temperature and pressure dependences of the dielectric constants of semiconductors. *Phys Rev B* 1983, 27:3494–3505
61. A. Ramzy, W. J. Aziz, Z. Hassan, *Optik-International Journal for Light and Electron Optics* 122 (2011): 2075-2077.
62. C. H. Chen, Y. F. Chen, *Solid State Commun.* 111 (1999): 681–685.
63. K. Omar, Z. Hassan, A. Ramzy, H. Abu Hassan, *JOAM* 11 (2009): 1641–1646.
64. S. L. Ossicini, P. F. Priolo, *Light Emitting Silicon for Microphotonics*, Springer, Germany, 38: (2003) 5726.
65. S. M. Sze, K. K. Ng, *Physics of Semiconductor Devices*, John Wiley & Sons, New Jersey (2003).